American Mineralogist, Volume 95, pages 724–735, 2010

Crystal chemistry of synthetic lawsonite solid-solution series $CaAl_2[(OH)_2/Si_2O_7]\cdot H_2O$–$SrAl_2[(OH)_2/Si_2O_7]\cdot H_2O$ and the *Cmcm*–*P*2_1/*m* phase transition

A. Liebscher,[1,2,*] G. Dörsam,[2] G. Franz,[2] B. Wunder,[3] and M. Gottschalk[3]

[1]Centre for CO_2 Storage, German Research Centre for Geosciences GFZ Potsdam, Telegrafenberg, D-14473 Potsdam, Germany
[2]Fachgebiet Mineralogie und Petrologie, Technische Universität Berlin, Ackerstrasse 76, D-13355 Berlin, Germany
[3]Section 3.3, Chemistry and Physics of Earth Materials, German Research Centre for Geosciences GFZ Potsdam, Telegrafenberg, D-14473 Potsdam, Germany

Abstract

Crystals of the solid-solution series of (Ca,Sr)-lawsonite were synthesized hydrothermally at 4 GPa and 600 and 800 °C in piston-cylinder experiments. Synthesis products were analyzed with SEM, EMP, and powder-XRD. Lawsonite was observed in both the orthorhombic space group *Cmcm* and in the monoclinic space group *P*2_1/*m*. It is exclusively orthorhombic at low x_{Sr}^{bulk} but monoclinic at high x_{Sr}^{bulk}; in the range x_{Sr}^{bulk} = 0.18 to 0.4 both polymorphs coexist and the data suggest a two-phase field between x_{Sr}^{ortho} ~0.1–0.2 and x_{Sr}^{mono} ~0.3–0.4 at 4 GPa/600 °C. Linear regression to the refined lattice parameters yields $a = 0.017\cdot x_{Sr} + 5.841$ (Å), $b = 0.197\cdot x_{Sr} + 8.787$ (Å), $c = 0.263\cdot x_{Sr} + 13.130$ (Å), and $v = 4.62\cdot x_{Sr} + 101.46$ (cm^3/mol) for orthorhombic lawsonite and $a = 0.119\cdot x_{Sr} + 5.306$ (Å), $b = 0.118\cdot x_{Sr} + 13.160$ (Å), $c = 0.025\cdot x_{Sr} + 5.833$ (Å), $\beta = 0.38\cdot x_{Sr} + 124.07$ (°), and $v = 3.20\cdot x_{Sr} + 101.59$ (cm^3/mol) for monoclinic lawsonite. The data suggest an increasingly negative $\Delta v_{ortho\text{-}mono}$ with increasing x_{Sr}. In monoclinic lawsonite, structural expansion due to the incorporation of Sr is primarily accomplished by tilting and rotation within the Si_2O_7-group, whereas in orthorhombic lawsonite this tilting and rotation is prohibited by symmetry restrictions and expansion is mostly accomplished by an increase in lattice parameters. Combining the extrapolated Ca end-member volume for monoclinic lawsonite with published high-*P* data yields K_0^{mono} = 137(3) GPa (K' = 4.4). Contrary to the Ca end-member system, the *Cmcm*–*P*2_1/*m* phase transition is quenchable within the Sr-bearing system. A tentative phase diagram for (Ca,Sr)-lawsonite at 600 °C indicates a narrow orthorhombic-monoclinic two-phase field that shifts significantly to lower pressure with increasing x_{Sr}. The *Cmcm*–*P*2_1/*m* phase transition in the Sr end-member system is located at ≤1 GPa at ~400 to 600 °C, 6 to 9 GPa below the transition in the Ca-system, and has a negative *P*-*T* slope.

Keywords: Crystal structure, lawsonite, XRD data, experimental petrology

Introduction

Lawsonite, $CaAl_2Si_2O_7(OH)_2\cdot H_2O$, an index mineral for high-pressure, low-temperature metamorphism, is common in blueschist-facies metabasalts and metagreywackes. It is stable up to extremely high pressure of 12 GPa (Schmidt 1995) and a potential carrier of H_2O into the Earth's depth in subduction zones. However, lawsonite is not only a carrier of H_2O but also of the geochemically important trace element Sr (among others) in high- and ultrahigh-pressure rocks, where it controls the whole-rock chemical budget of Sr (Tribuzio et al. 1996; Zack et al. 2002; Spandler et al. 2003). Therefore, understanding the geochemical cycle of Sr during metamorphism and especially within subduction zones requires understanding of its crystal-chemical incorporation in lawsonite.

At ambient conditions, lawsonite and its Sr-analog itoigawaite, $SrAl_2Si_2O_7(OH)_2\cdot H_2O$, are both orthorhombic with space group *Cmcm* (Fig. 1a; Baur 1978; Miyajima et al. 1999). The structure is composed of single chains of edge-sharing octahedra (M site) parallel [100]. The M site is occupied by trivalent cations, preferentially by Al. Kinked Si_2O_7-groups bridge the octahedral chains in [010] and [001]; within this framework one relatively large A position forms, which is occupied by the large divalent cations Ca and Sr. Several *P*-*T* induced phase transitions have been determined for lawsonite. At low temperatures, its space group reduces to *Pmcn* below 273 K/0.1 MPa and to *P*2_1*cn* below 155 K/0.1 MPa (Libowitzky and Armbruster 1995; Meyer et al. 2000, 2001; Martin-Olalla et al. 2001). These reversible phase transitions are mainly caused by shifts of the OH-group and H_2O from highly symmetric to ordered positions at low temperatures. At high pressure/room temperature, a reversible and non-quenchable phase transition from orthorhombic *Cmcm* to monoclinic *P*2_1/*m* (*C*11_2/*m*) lawsonite occurs at ~8.6 GPa (Scott and Williams 1999; Daniel et al. 2000). This phase transition was also observed by Pawley and Allan (2001), however, at slightly higher pressure of ~10 to 11 GPa/room temperature. The latter authors explained the phase transition by shearing of $(010)_{ortho}$ planes in $[100]_{ortho}$ (Fig. 1b). As a consequence, monoclinic *P*2_1/*m* lawsonite has two different octahedral sites M1 and M2, slightly distorted Si_2O_7-groups, and the lattice parameters of the two polymorphs are related to each other by $2a_{mono}\sin\beta_{mono} = b_{ortho}$, $b_{mono} = c_{ortho}$, and $c_{mono} = a_{ortho}$. Boffa-Ballaran and Angel (2003) pressurized lawsonite up to 9.82 GPa/room temperature and tested the *C*-centering with ω-scans of the (017) reflection, which is absent in *Cmcm* space group. Above 4 GPa/room tem-

* E-mail: alieb@gfz-potsdam.de

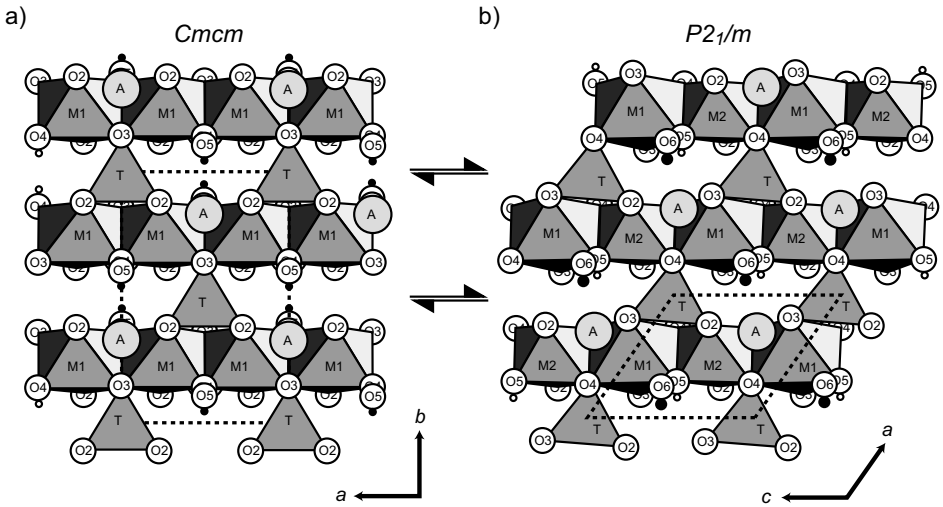

FIGURE 1. Comparison of the orthorhombic *Cmcm* (**a**) and monoclinic $P2_1/m$ (**b**) lawsonite structure, projected onto the *a*-*b* and *a*-*c* plane, respectively. Dotted line is outline of the elementary cell. Hydrogen atoms are shown as small circles for the OH-group at $O4_{ortho}$ and $O5_{mono}$ and as dots for the H_2O molecule at $O5_{ortho}$ and $O6_{mono}$. The transition from *Cmcm* to $P2_1/m$ is marked by tilting and rotation of the tetrahedra of the Si_2O_7-groups, shearing of $(010)_{ortho}$ in $[100]_{ortho}$, and splitting of $M1_{ortho}$ into $M1_{mono}$ and $M2_{mono}$ and of $O2_{ortho}$ into $O2_{mono}$ and $O3_{mono}$.

perature, low intensities of the (017) reflection indicate a phase transition from *Cmcm* to a primitive orthorhombic cell, most likely *Pmcn* or $P2_1cn$; final transition to $P2_1/m$ was determined at 9.5 GPa, intermediate between the results of Daniel et al. (2000) and Pawley and Allan (2001).

Chemical variations in the lawsonite mineral group and potential solid-solutions series are indicated by the minerals itoigawaite $SrAl_2Si_2O_7(OH)_2 \cdot H_2O$ (*Cmcm*; Miyajima et al. 1999), hennomartinite $SrMn_2Si_2O_7(OH)_2 \cdot H_2O$ ($P2_1cn$; Armbruster et al. 1992), and noélbensonite $BaMn_2Si_2O_7(OH)_2 \cdot H_2O$ (*Cmcm*; Kawachi et al. 1996). Because itoigawaite and lawsonite have identical space group at ambient conditions, the assumption of a complete Ca-Sr solid-solution series between both end-members is reasonable. Hennomartinite, on the other hand, shows phase transitions that are comparable to those found in lawsonite (Libowitzky and Rossman 1996). It is, therefore, likely that phase transitions observed for the end-members lawsonite and hennomartinite are not only induced by *P* and *T* but also by major element substitutions along the potential solid-solution series.

Here we present systematic experimental data on the $Ca_{-1}Sr_{+1}$ substitution within the (Ca,Sr)-lawsonite solid-solution series. Minerals were synthesized in the presence of an aqueous (Ca,Sr)Cl_2-solution at 4 GPa/600 and 800 °C. We show that: (1) at 4 GPa/600 and 800 °C, the high-pressure polymorph of itoigawaite is monoclinic with space group $P2_1/m$; (2) incorporation of the larger Sr for Ca induces the orthorhombic to monoclinic phase transition; (3) there is a two-phase field in which orthorhombic and monoclinic (Ca,Sr)-lawsonite coexist; and (4) substitution of Sr for Ca notably enlarges the stability field of monoclinic lawsonite toward lower pressure.

EXPERIMENTAL AND ANALYTICAL METHODS

Experimental techniques

Starting materials were oxide-hydroxide mixtures of α-quartz, γ-Al_2O_3, $Ca(OH)_2$, and $SrSiO_3$ (prepared from $SrCO_3$ plus quartz by heating for ≈24 h at 1100 °C) weighed in stoichiometric amounts of the desired $(Ca,Sr)Al_2Si_2O_7(OH)_2 \cdot H_2O$ composition (Table 1). For the Sr end-member, we used $Sr(OH)_2 \cdot 8H_2O$ instead of $SrSiO_3$. Excess SiO_2 (~3.0 mol%) was added to each run to account for preferred dissolution of SiO_2 into the fluid. The Ca-Sr composition of the solid starting material (bulk) ranges from $x_{Sr}^{bulk} = 0.02$ to 1.00, where $x_{Sr}^{bulk} = Sr/(Sr+Ca)$. Following Zimmermann et al. (1996), a 1 *M* (Ca,Sr)Cl_2 aqueous solution with x_{Sr} identical to x_{Sr}^{bulk} was added to overcome kinetic problems. The initial $(Sr+Ca)^{fluid}/[(Sr+Ca)^{fluid} + (Sr+Ca)^{solid}]$ ratio varies between 0.045 and 0.141.

The starting mixtures of solids and fluid were sealed in Au capsules (except for the Sr end-member synthesis, which was run in a Pt capsule) of 10 to 13 × 2 mm with a wall thickness of 0.115 mm. Four capsules were run in a common assembly at a time. Experiments were performed at 4.0 GPa/600 and 800 °C for 4 to 7 days, using a standard piston-cylinder apparatus with NaCl assembly and steel furnace. The temperature was recorded online with an accuracy of ±10 °C, based on our in-house calibration, using a Ni-CrNi thermocouple placed closely adjoining the center of the capsules. Pressure was controlled within ±50 MPa. The assembly was first pressurized to 3.0 GPa, then heated to 600 or 800 °C and finally pressurized to 4.0 GPa. After quenching, the capsules were cleaned, weight checked, and opened in distilled H_2O to recover the run fluid. Solid run products were dried at 100 °C for 15 min.

Analytical methods

SEM images of the synthesis products were obtained with a Hitachi-S2700 instrument. EMP analyses were performed on polished and carbon-coated samples with a Cameca SX 50 microprobe using wavelength dispersive spectrometry and the PAP correction program (Pouchou and Pichoir 1984). Acceleration voltage was 10 kV, beam current 15.2 nA, and beam diameter was 1 µm. Counting time for all elements was 16 s on the peak position and the background was measured for 8 s on each side of the peak. TAP analyzer crystals were used for Sr*L*β, Si*K*β, and Al*K*α and a PET crystal for Ca*K*α. Standards employed were synthetic wollastonite (Si and Ca) and synthetic $SrAl_2Si_2O_8$ (Al and Sr).

For XRD with Rietveld refinement, sub-samples of the run products were ground in an agate mortar for several minutes, diluted with plain white glue and then evenly spread on a circular foil. During drying, the powder was stirred to minimize preferred orientation. The foil was covered with a second foil and placed into the transmission sample holder. Powder XRD patterns were recorded in transmission between $2\Theta = 5$ and 125° using a fully automated STOE STADI-P diffractometer with Cu$K\alpha_1$ radiation equipped with a primary monochromator and a 7° wide position sensitive detector (PSD). The normal-focus Cu X-ray tube was operated at 40 kV and 40 mA, using a take-off angle of 6°. We used a detector step size of 0.1° and a resolution of $2\Theta = 0.01°$. Phase proportions, unit-cell and other structural parameters were refined using the GSAS software package for Rietveld refinement (Larson and Von Dreele 1987). The peaks were defined as pseudo-Voigt with variable Lorentzian character. The peak full-width at half

TABLE 1. Starting compositions for (Ca,Sr)-lawsonite synthesis and results of quantitative phase analyses by Rietveld refinement of powder-XRD data; run conditions are 600 °C/4.0 GPa (800 °C/4.0 GPa for Pt100), 4–7 days run duration, 1 *M* $(Ca,Sr)Cl_2$ solution

Run	Au76	Au77	Au78	Au79	Au63	Au62	Au83	Au86
x_{Sr}^{bulk}	0.02	0.03	0.04	0.05	0.18	0.249	0.25	0.4
SiO_2 (mg)	12.23	12.11	12.36	12.26	9.57	9.24	11.07	8.47
Al_2O_3 (mg)	9.74	9.70	9.94	9.91	8.69	8.71	9.88	8.21
$Ca(OH)_2$ (mg)	6.94	6.83	6.93	6.84	5.18	4.75	5.39	3.58
$SrSiO_3$ (mg)*	0.31	0.47	0.64	0.79	2.51	3.47	3.97	5.27
solid total (mg)	29.229	29.112	29.876	29.801	25.94	26.17	30.305	25.534
fluid total (mg)	11.013	11.173	9.333	10.957	5.11	4.37	15.796	10.774
$(Ca+Sr)^{fluid}/(Ca+Sr)^{total}$	0.096	0.098	0.081	0.094	0.052	0.045	0.129	0.108
Quantitative phase analyses (wt%)†								
lawsonite $P2_1/m$	/	/	/	/	57	69	58	87
lawsonite *Cmcm*	95	93	95	96	42	28	38	6
coesite	5	7	5	4	/	1	4	7
grossular	/	/	/	/	1	/	/	/
Refinement statistics								
fitted wR_p	0.098	0.080	0.073	0.085	0.047	0.067	0.064	0.056
variables	96	88	92	94	98	120	124	133
χ^2	1.228	1.250	1.167	1.417	1.187	1.977	1.135	1.384
DWd	1.302	1.200	1.338	1.080	1.335	0.807	1.335	1.097

Run	Au87	Au82	Au91	Au47	Au92	Au88	Au89	Pt100
x_{Sr}^{bulk}	0.45	0.5	0.625	0.65	0.75	0.75	0.875	1.0
SiO_2 (mg)	8.54	9.51	6.31	5.17	5.99	5.72	5.14	4.36
Al_2O_3 (mg)	8.53	9.78	7.51	5.85	7.82	7.47	7.42	3.65
$Ca(OH)_2$ (mg)	3.41	3.55	2.04	1.49	1.42	1.36	0.67	–
$SrSiO_3$ (mg)*	6.16	7.85	7.50	6.11	9.42	8.99	10.42	9.50
solid total (mg)	26.64	30.689	23.37	18.624	24.65	23.54	23.648	17.50
fluid total (mg)	10.872	10.769	8.14	5.539	4.41	13.511	9.79	5.11
$(Ca+Sr)^{fluid}/(Ca+Sr)^{total}$	0.105	0.092	0.090	0.079	0.049	0.141	0.107	–
Quantitative phase analyses (wt%)†								
lawsonite $P2_1/m$	95	96	93	93	82	90	94	75
lawsonite *Cmcm*	/	/	/	/	/	/	/	/
coesite	5	4	/	7	/	/	1	/
grossular	/	/	4	/	4	10	2	/
Refinement statistics								
fitted wR_p	0.059	0.071	0.069	0.056	0.073	0.072	0.074	0.045
variables	78	81	90	82	92	72	88	91
χ^2	1.542	1.615	1.883	2.556	1.664	1.241	1.186	1.226
DWd	1.006	0.955	0.845	0.666	0.961	1.260	1.351	1.246

Note: Additional phases: 1 wt% kyanite and wollastonite each in Au62; 3 wt% strontianite in Au91; 13 wt% zoisite in Au92; 1 wt% strontianite and 2 wt% wollastonite in Au89; 25 wt% strontianite in Pt100.
* Except for Pt100 for which $Sr(OH)_2 \cdot 8H_2O$ was used.
† Error on quantitative phase analyses $2\sigma < 1$ wt%.

maximum height was varied as a function of 2Θ using the parameters U, V, and W of Caglioti et al. (1958). For the Lorentzian character, the parameters X and Y were used. Because of the geometry of the STADIP diffractometer, the recorded reflections are highly symmetric and no parameters describing the asymmetry of the peaks had to be used. To model the diffuse background from the amorphous foil and glue used for the preparation, the background was fitted with a real space correlation function. Refinements were done in space groups $P2_1/m$ for monoclinic (Ca,Sr)-lawsonite and *Cmcm* for orthorhombic (Ca,Sr)-lawsonite, and they were started with the structural data by Pawley and Allan (2001) for monoclinic lawsonite and Libowitzky and Armbruster (1995) for orthorhombic lawsonite. The atomic displacement parameters were fixed at the values from Libowitzky and Armbruster (1995).

The refinements were performed in the following sequence: scale factor, background, zero-point correction, phase fractions, lattice parameters, preferred orientation, profile parameter Caglioti W and Lorentz X, fractional atom coordinates for monoclinic and orthorhombic lawsonite (except for hydrogen), site occupancy of lawsonite A-site, and remaining profile parameters Caglioti U and V and Lorentz Y.

RESULTS

Description of run products

Weight fractions and structural parameters of the solid run products were refined successfully in all runs (Table 1): χ^2 varies between 1.135 and 2.556 and DWd between 0.666 and 1.351. All runs contain 75 to 99 wt% lawsonite and variable amounts of coesite (1 to 7 wt%) and/or grossular (1 to 10 wt%) except for Pt100 that lack both coesite and grossular. Additional phases are kyanite in Au62, wollastonite in Au62 and Au89, strontianite in Au91, Au89, and Pt100, and zoisite in Au92. Lawsonite forms small euhedral crystals, the size of which is mostly below 10 μm; at low x_{Sr}^{bulk} its habit is more prismatic, while at higher x_{Sr}^{bulk} it is more isometric (Fig. 2).

The refinements show that lawsonite occurs in both the orthorhombic *Cmcm* and monoclinic $P2_1/m$ form depending on x_{Sr}^{bulk}: it is exclusively orthorhombic in runs at $x_{Sr}^{bulk} < 0.18$ but exclusively monoclinic at $x_{Sr}^{bulk} > 0.4$; in the range $x_{Sr}^{bulk} = 0.18$ to 0.4 both polymorphs coexist and the data suggest that within this compositional range the amount of orthorhombic lawsonite decreases, while that of monoclinic lawsonite increases with increasing x_{Sr}^{bulk}. The corresponding change of the powder-XRD patterns with increasing x_{Sr}^{bulk} is exemplified in Figure 3 for $2\theta = 12$ to 28°: up to $x_{Sr}^{bulk} = 0.05$ only distinct, orthorhombic peaks are observed. At $x_{Sr}^{bulk} = 0.18$ to 0.4, where both orthorhombic and monoclinic lawsonite coexist, peaks broaden and orthorhombic and monoclinic peaks overlap; at $x_{Sr}^{bulk} > 0.4$ only monoclinic peaks are observed with a clear peak splitting of $(110)_{orth}$, $(111)_{orth}$, $(112)_{orth}$, and $(113)_{orth}$. Un-split peaks $(002)_{orth}/(020)_{mcl}$, $(021)_{orth}/(011)_{mcl}$, and $(022)_{orth}/(021)_{mcl}$ generally shift to lower 2θ values with increasing x_{Sr}^{bulk}.

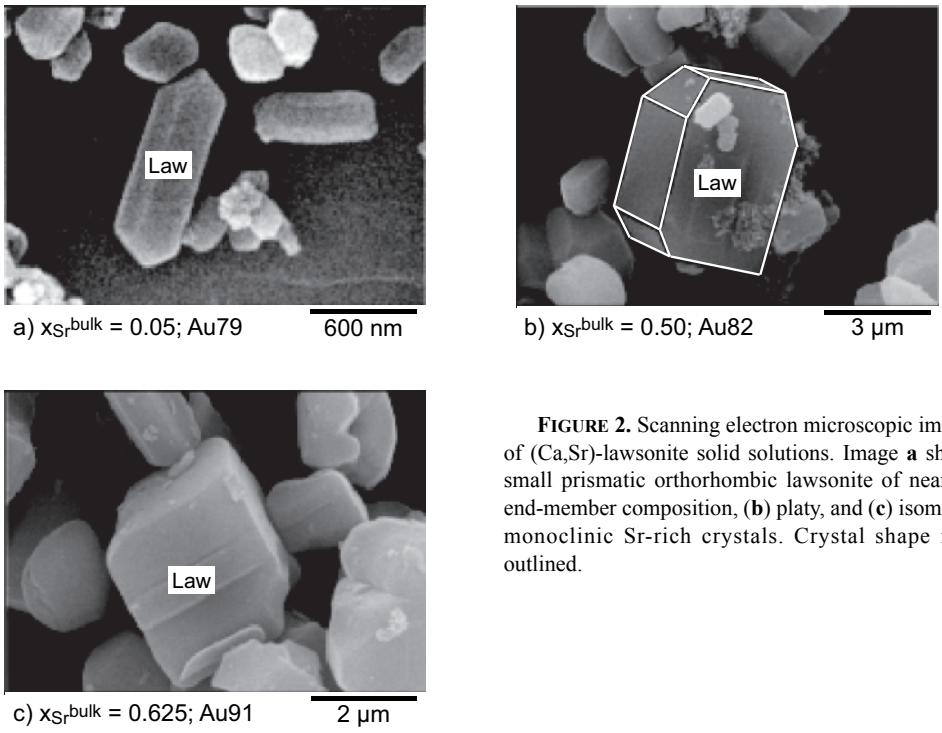

FIGURE 2. Scanning electron microscopic images of (Ca,Sr)-lawsonite solid solutions. Image **a** shows small prismatic orthorhombic lawsonite of near Ca end-member composition, (**b**) platy, and (**c**) isometric monoclinic Sr-rich crystals. Crystal shape in **b** outlined.

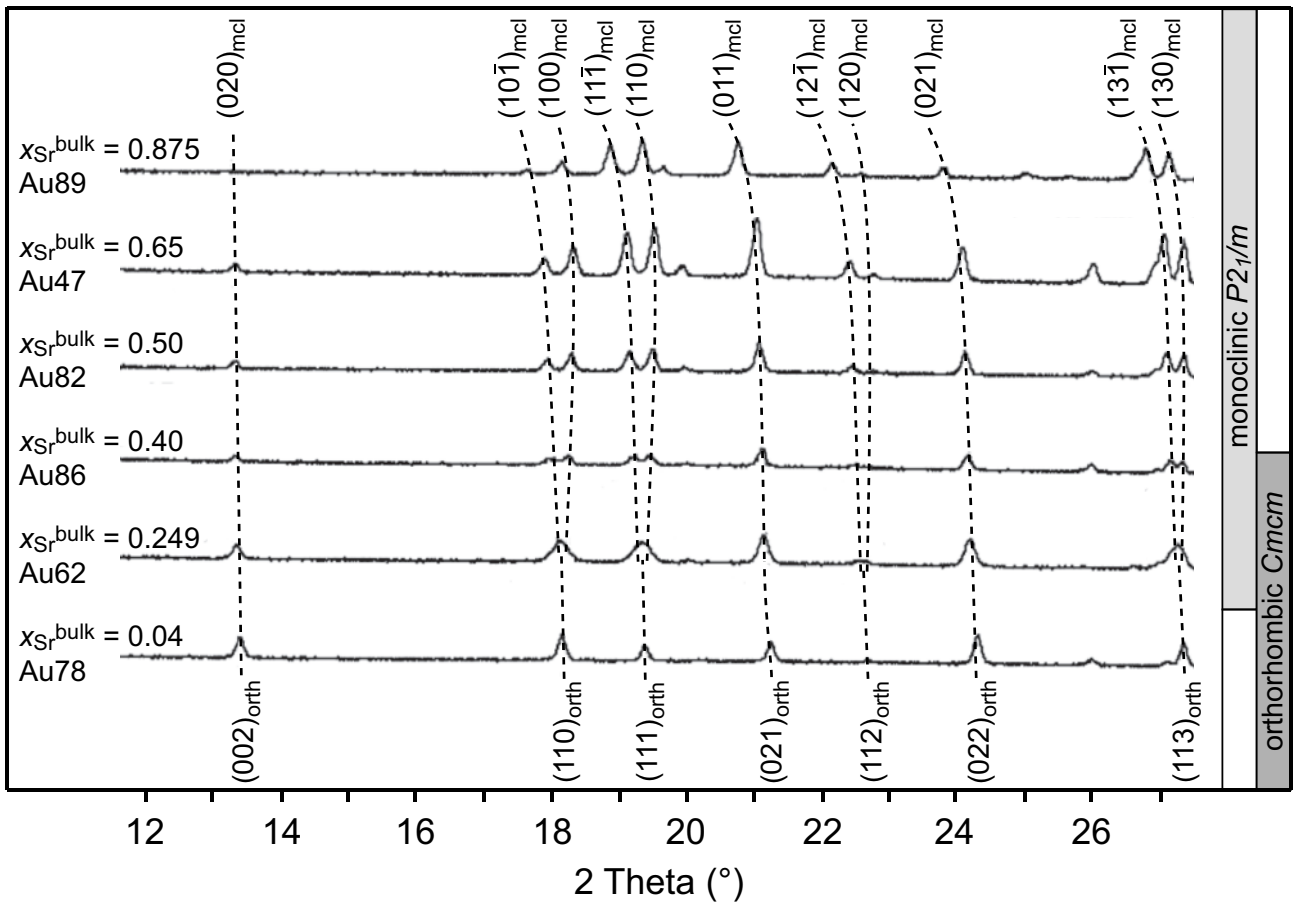

FIGURE 3. Selected powder-XRD pattern of run products between 12° and 28° 2θ. Monoclinic (Ca,Sr)-lawsonite solid solutions are characterized by peak splitting and peak shift compared to orthorhombic lawsonite. Runs Au62 at x_{Sr}^{bulk} = 0.249 and Au86 at x_{Sr}^{bulk} = 0.40 are examples for coexisting monoclinic and orthorhombic lawsonite.

TABLE 2. Average chemical composition (wt%) as determined by EMP analyses and calculated structural formulae of orthorhombic and monoclinic (Ca,Sr)-lawsonite solid solutions

Run	Au76	Au77	Au78	Au79	Au63	Au62	Au83	Au86
x_{Sr}^{bulk}	0.02	0.03	0.04	0.05	0.18	0.249	0.25	0.4
Space group	*Cmcm*	*Cmcm*	*Cmcm*	*Cmcm*	*Cmcm*, $P2_1/m$	*Cmcm*, $P2_1/m$	*Cmcm*, $P2_1/m$	$P2_1/m$
N	31	64	26	28	25	189	18	16
SiO_2	38.21(25)	38.20(19)	38.14(81)	37.89(57)	37.11(38)	35.97(76)	37.88(27)	36.62(63)
Al_2O_3	32.11(26)	31.95(28)	31.90(49)	31.96(48)	30.95(51)	30.41(66)	31.49(26)	30.72(49)
CaO	17.05(17)	16.90(17)	16.35(35)	16.67(40)	12.46(60)	11.57(1.76)	13.68(60)	10.29(31)
SrO	0.53(5)	0.73(7)	0.99(10)	1.26(9)	7.23(89)	9.30(1.24)	6.49(75)	11.53(52)
Total	87.9(5)	87.79(39)	87.4(1.3)	87.8(1.4)	87.75(64)	87.26(1.56)	89.04(52)	89.2(1.1)
Structural formulae on basis of 8 O atoms								
Si	2.01(1)	2.02(1)	2.02(2)	2.01(1)	2.03(1)	2.01(2)	2.01(1)	2.02(2)
Al	2.00(1)	1.99(1)	2.00(2)	2.00(1)	1.99(2)	2.00(4)	1.99(2)	1.99(2)
Ca	0.96(1)	0.96(1)	0.93(2)	0.95(1)	0.73(3)	0.69(9)	0.79(3)	0.61(2)
Sr	0.02(1)	0.02(1)	0.03(2)	0.04(1)	0.23(3)	0.30(4)	0.20(2)	0.37(2)
Ca+Sr	0.98(1)	0.98(1)	0.96(2)	0.99(1)	0.96(2)	0.99(7)	0.99(1)	0.98(1)
x_{Sr}	0.016(2)	0.023(2)	0.03(1)	0.04(1)	0.24(3)	0.30(4)	0.20(3)	0.38(2)

Run	Au87	Au82	Au91	Au47	Au92	Au88	Au89
x_{Sr}^{bulk}	0.45	0.5	0.625	0.65	0.75	0.75	0.875
Space group	$P2_1/m$	$P2_1/m$	$P2_1/m$	$P2_1/m$	$P2_1/m$	$P2_1/m$	$P2_1/m$
N	22	24	24	26	17	9	11
SiO_2	36.19(53)	35.17(55)	34.53(35)	34.82(29)	33.00(46)	33.00(42)	33.1(1.2)
Al_2O_3	30.27(60)	29.73(39)	28.99(40)	29.32(36)	27.88(19)	27.27(55)	27.38(98)
CaO	9.16(42)	8.05(48)	4.06(37)	5.64(23)	0.97(43)	0.89(38)	0.36(5)
SrO	13.20(59)	14.76(82)	21.68(86)	19.01(48)	26.72(54)	26.86(60)	27.78(66)
Total	88.8(1.3)	87.7(1.1)	89.27(84)	88.79(67)	88.56(78)	88.0(1.4)	88.6(1.9)
Structural formulae on basis of 8 O atoms							
Si	2.02(1)	2.01(1)	2.01(1)	2.01(1)	2.00(1)	2.02(1)	2.02(2)
Al	1.99(1)	2.00(1)	1.99(2)	2.00(2)	1.99(2)	1.97(1)	1.97(2)
Ca	0.55(2)	0.49(3)	0.25(2)	0.35(1)	0.06(3)	0.06(2)	0.02(1)
Sr	0.43(2)	0.49(3)	0.73(3)	0.64(2)	0.94(2)	0.95(2)	0.98(4)
Ca+Sr	0.98(1)	0.98(2)	0.98(2)	0.99(1)	1.00(2)	1.01(1)	1.00(4)
x_{Sr}	0.44(2)	0.50(3)	0.74(2)	0.65(1)	0.94(1)	0.94(2)	0.98(1)

Notes: Au63, Au62, and Au83 contain both polymorphs and unequivocal assignment of EMP analyses to either of both was impossible. Au86 contains only 6 wt% orthorhombic lawsonite (see Table 1), and it is assumed that this amount does not bias the determined composition of the major phase monoclinic lawsonite; *N* number of EMP point analyses; errors in parentheses refer to mean standard deviation 1σ; x_{Sr} = Sr/(Sr+Ca).

Composition of solid run products

Despite its generally small crystal size, lawsonite could be analyzed by EMP (Table 2). In runs Au62, Au63, and Au83, which contain almost equal amounts of orthorhombic and monoclinic lawsonite, no unequivocal assignment of the EMP analyses to either form could be made, which makes a reliable interpretation of these EMP analyses impossible; for Au86 with only 6 wt% orthorhombic lawsonite, it is assumed that this amount does not bias the determined composition of the major phase monoclinic lawsonite. Based on the EMP data, we have no hints for any compositional zoning in lawsonite, neither in individual crystals nor between different crystals within the individual runs. Grossular could be analyzed in runs Au88 and Au89; it contains only small amounts of Sr and calculated $x_{Sr}^{grossular}$ are 0.016 and 0.045, respectively. Strontianite could be analyzed in run Au89 and has $x_{Sr}^{strontianite} = 0.97$.

Refined $x_{Sr}^{lawsonite}$ values based on XRD measurements (Table 3) agree well with the EMP results except for runs Au62, Au63, and Au83, in which EMP analyses could not distinguish between orthorhombic and monoclinic lawsonite (Fig. 4a). In these runs, the XRD data clearly show higher x_{Sr}-values in monoclinic than in coexisting orthorhombic (Ca,Sr)-lawsonite indicating a two-phase field where Sr-poor orthorhombic and Sr-rich monoclinic lawsonite coexist. Given the overall good agreement between EMP and XRD results, we will refer only to the XRD data in the following. Calculated $x_{Sr}^{lawsonite}$ generally corresponds to x_{Sr}^{bulk} of the respective runs; only in runs Au91, Au92, Au88, and Au89, which contain grossular, $x_{Sr}^{lawsonite}$ is notably higher than x_{Sr}^{bulk} (Fig. 4b).

Structural changes in monoclinic and orthorhombic lawsonite with x_{Sr}

Lattice parameters. Refined lattice parameters a_{mono}, b_{mono}, c_{mono}, and β_{mono} depend almost linearly on x_{Sr} at $x_{Sr} > 0.4$, but deviate clearly from this linear trend below $x_{Sr} = 0.4$, where monoclinic and orthorhombic lawsonite coexist (Table 3a; Fig. 5). Despite the overall non-linear behavior of a_{mono}, b_{mono}, c_{mono}, and β_{mono}, calculated v_{mono} depends linearly on x_{Sr} (Table 3a; Fig. 5d). The change in compositional dependency of a_{mono}, b_{mono}, c_{mono}, and β_{mono} below $x_{Sr} = 0.4$ indicates a change in structural response to the volume decrease toward low x_{Sr} and may suggest increasing strain within the monoclinic structure. To derive the compositional dependency of the lattice parameters of strain-free monoclinic lawsonite, we tentatively fitted the data at $x_{Sr} > 0.4$ with linear regressions to

$a = 0.119 \cdot x_{Sr} + 5.306$ (Å),
$b = 0.118 \cdot x_{Sr} + 13.160$ (Å),
$c = 0.025 \cdot x_{Sr} + 5.833$ (Å),
$\beta = 0.38 \cdot x_{Sr} + 124.07$ (°),
$v = 3.20 \cdot x_{Sr} + 101.59$ (cm³/mol) (Fig. 5).

Refined x_{Sr} of orthorhombic lawsonite from runs Au63, Au62, and Au83 have large uncertainties and the compositional dependency of refined lattice parameters a_{ortho}, b_{ortho}, c_{ortho}, and calculated v_{ortho} are less well constrained. The data nevertheless are consistent with linear dependencies of a_{ortho}, b_{ortho}, c_{ortho}, and v_{ortho} on x_{Sr} (Fig. 5). Linear regression yields

$a = 0.017 \cdot x_{Sr} + 5.841$ (Å),

TABLE 3a. Refined Sr-Ca composition and lattice parameters of monoclinic (Ca,Sr)-lawsonite

Run	Au63	Au62	Au83	Au86	Au87	Au82
x_{Sr}	0.21(4)	0.320(18)	0.23(4)	0.36(2)	0.41(2)	0.493(12)
a (Å)	5.3032(14)	5.3300(9)	5.3025(11)	5.3427(6)	5.3510(5)	5.3640(3)
b (Å)	13.174(3)	13.1956(14)	13.174(2)	13.2039(9)	13.2073(9)	13.2175(5)
c (Å)	5.8436(16)	5.8449(10)	5.8422(10)	5.8448(6)	5.8443(4)	5.8452(3)
β (°)	123.76(2)	123.96(1)	123.72(1)	124.10(1)	124.17(1)	124.25(1)
V (Å^3)	339.39(7)	340.97(9)	339.52(7)	341.41(4)	341.73(5)	342.55(3)
Run	Au91	Au47	Au92	Au88	Au89	Pt100
x_{Sr}	0.727(18)	0.625(12)	0.966(18)	0.96(2)	0.981(12)	1.00
a (Å)	5.3962(4)	5.3849(2)	5.4205(2)	5.4194(2)	5.4222(2)	5.4231(2)
b (Å)	13.2461(7)	13.2377(4)	13.2735(4)	13.2737(5)	13.2778(5)	13.2761(4)
c (Å)	5.8505(4)	5.8489(2)	5.8573(2)	5.8575(2)	5.8584(2)	5.8583(3)
β (°)	124.39(1)	124.35(1)	124.43(1)	124.42(1)	124.42(1)	124.42(1)
V (Å^3)	345.11(4)	344.225(18)	347.61(2)	347.59(2)	347.93(2)	347.95(2)

Notes: Refinements in space group $P2_1/m$. Z = 2; errors in parentheses refer to 2σ.

TABLE 3b. Refined Sr-Ca composition and lattice parameters of orthorhombic (Ca,Sr)-lawsonite

Run	Au76	Au77	Au78	Au79	Au63	Au62	Au83	Au86*
x_{Sr}	0.018(12)	0.029(12)	0.035(18)	0.021(12)	0.111(43)	0.193(3)	0.18(4)	
a (Å)	5.8422(2)	5.8417(2)	5.8415(2)	5.8419(2)	5.8439(5)	5.8457(5)	5.8433(4)	5.8442(9)
b (Å)	8.7904(4)	8.7904(4)	8.7916(4)	8.7940(4)	8.8112(13)	8.8286(13)	8.8169(8)	8.858(4)
c (Å)	13.1344(5)	13.1345(4)	13.1360(5)	13.1393(5)	13.1618(19)	13.1834(17)	13.1726(11)	13.199(4)
V (Å^3)	674.52(5)	674.47(5)	674.62(5)	675.01(5)	677.72(14)	680.39(14)	678.64(10)	683.3(3)

Notes: Refinements in space group *Cmcm*. Z = 4; errors in parentheses refer to 2σ.
* Refinement of x_{Sr} not successful.

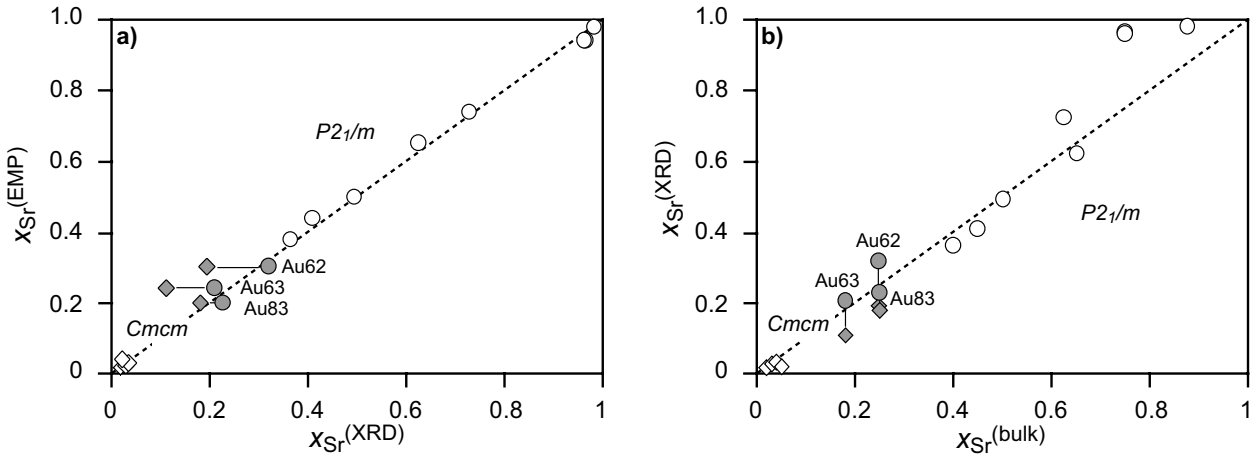

FIGURE 4. (**a**) Composition of orthorhombic and monoclinic lawsonite as determined by EMP and XRD analyses. In runs Au62, Au63, and Au83, EMP analyses could not distinguish between orthorhombic and monoclinic lawsonite. For these runs, XRD data indicate $x_{Sr}^{ortho} < x_{Sr}^{mono}$. (**b**) Comparison between orthorhombic and monoclinic lawsonite composition as determined by XRD analyses and corresponding x_{Sr}^{bulk} (diamonds: orthorhombic lawsonite, circles: monoclinic lawsonite, filled symbols: runs with coexisting orthorhombic and monoclinic lawsonite).

$b = 0.197 \cdot x_{Sr} + 8.787$ (Å),
$c = 0.263 \cdot x_{Sr} + 13.130$ (Å),
$v = 4.62 \cdot x_{Sr} + 101.46$ (cm^3/mol).

The extrapolated orthorhombic Ca end-member values b = 8.787 Å and c = 13.130 Å agree with data reported in the literature, whereas a = 5.841 Å is notably and v = 101.46 cm^3/mol slightly smaller than the corresponding literature values (Fig. 5; Baur 1978; Libowitzky and Armbruster 1995; Comodi and Zanazzi 1996; Meyer et al. 2001). The extrapolated orthorhombic Sr end-member values a = 5.858 Å, b = 8.984 Å, c = 13.393 Å, and v = 106.08 cm^3/mol generally differ from those reported for itoigawaite of a = 6.031 Å, b = 8.945 Å, c = 13.219 Å, and v = 107.40 cm^3/mol (Miyajima et al. 1999). The reason for this discrepancy is not clear.

All lattice parameters of both polymorphs increase with increasing x_{Sr}, reflecting expansion of the structures due to substitution of the larger Sr for Ca. However, absolute values as well as compositional dependency of equivalent lattice parameters differ between both polymorphs, which are most obvious for a_{ortho} vs. c_{mono} and c_{ortho} vs. b_{mono} (Fig. 5). Due to these differences our data indicate $v_{ortho} \leq v_{mono}$ at low x_{Sr} and $v_{ortho} > v_{mono}$ at $x_{Sr} > 0.15$. Contrary, literature data (Baur 1978; Libowitzky and Armbruster 1995; Comodi and Zanazzi 1996; Meyer et al. 2001) suggest $v_{ortho} > v_{mono}$ even at low x_{Sr} (Fig. 5), which would be consistent with monoclinic Ca-lawsonite being the high-pressure polymorph and that is, therefore, more likely. Given the slight scatter and therefore low precision of our orthorhombic data, the exact volume relations between orthorhombic and monoclinic lawsonite at low x_{Sr} cannot be determined. But regardless of the

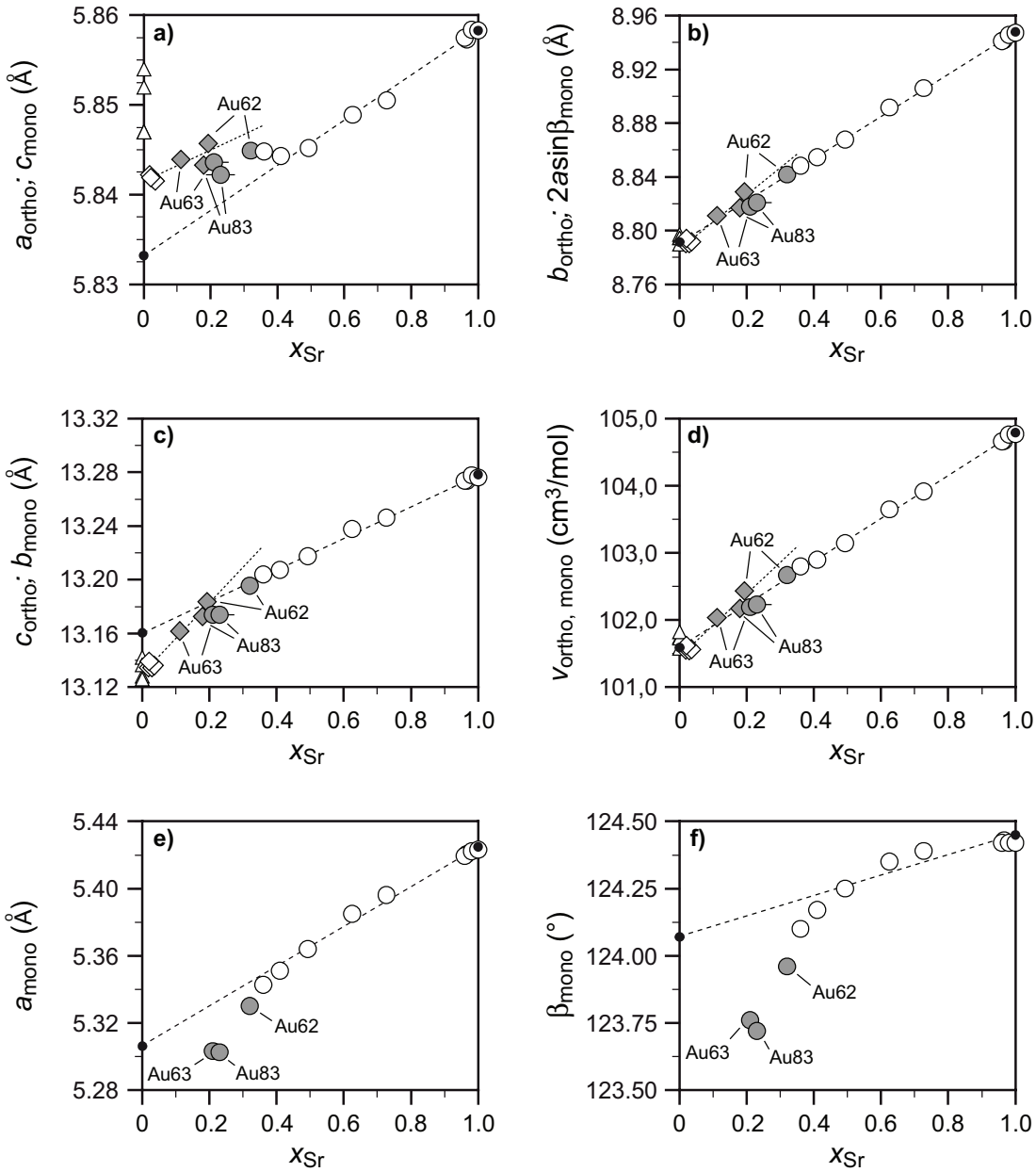

FIGURE 5. Refined lattice parameters of synthetic orthorhombic and monoclinic (Ca,Sr)-lawsonite with comparison to literature values for orthorhombic end-member lawsonite. Monoclinic lattice parameters display overall non-linear dependency on x_{Sr}, which is most pronounced at x_{Sr} < 0.4 but only minor at x_{Sr} > 0.4. Calculated v_{mono} (**d**) shows linear dependency on x_{Sr}. Dashed lines are tentative linear fits to the monoclinic data at x_{Sr} > 0.4 (see text). Orthorhombic lattice parameters slightly scatter but are consistent with a linear dependency on x_{Sr} (dotted lines). Extrapolated b_{ortho} and c_{ortho} agree well with the literature values, whereas a_{ortho} is notably and v_{ortho} slightly smaller [diamonds = orthorhombic lawsonite, circles = monoclinic lawsonite, filled symbols = runs with coexisting orthorhombic and monoclinic lawsonite, dots = extrapolated monoclinic end-member, triangles = literature values for orthorhombic end-member from Baur (1978), Libowitzky and Armbruster (1995), Comodi and Zanazzi (1996), and Meyer et al. (2001)].

exact volume relations at low x_{Sr}, the overall data suggest an increasingly negative $\Delta v_{ortho\text{-}mono}$ with increasing x_{Sr}.

Fractional atom coordinates. Refined fractional atom coordinates of both monoclinic and orthorhombic lawsonite display smooth, mostly linear shifts with x_{Sr} for most atoms (Table 4). Some refined fractional atom coordinates from runs Au63, Au62, Au83, and Au86 are, however, off the trends defined by the other runs and indicate less accurate refinement of fractional atom coordinates in these runs due to the coexistence of both polymorphs.

A-polyhedra. The A site in monoclinic lawsonite may be described as eight- to ninefold coordinated depending on the chosen cut-off value and x_{Sr}. With increasing x_{Sr}, the distance to a ninth oxygen (labled O6′) decreases linearly from ~3.31 Å at x_{Sr} ~0.2 to ~2.92 Å in Sr end-member lawsonite, so that in Sr-rich lawsonite the A-site should best be described as ninefold coordinated (Fig. 6a). Except for this bond to O6′, all other bonds

TABLE 4a. Refined fractional atomic coordinates of monoclinic (Ca-Sr)-lawsonite

Run		Au63	Au62	Au83	Au86	Au87	Au82	Au91	Au47	Au92	Au88	Au89	Pt100
x_{Sr}		0.21(4)	0.320(18)	0.23(4)	0.36(2)	0.41(2)	0.493(12)	0.727(18)	0.625(12)	0.966(18)	0.96(2)	0.981(12)	1.00
A	x	0.342(2)	0.3409(8)	0.340(1)	0.3431(9)	0.343(1)	0.3428(5)	0.3463(5)	0.3441(4)	0.3454(4)	0.3456(5)	0.3462(5)	0.3456(5)
	y				0.75						0.75		
	z	0.672(2)	0.6721(8)	0.671(1)	0.6772(9)	0.679(1)	0.6802(5)	0.6837(5)	0.6834(4)	0.6860(4)	0.6855(4)	0.6860(5)	0.6858(5)
M1	x				0.5						0.5		
	y				0						0		
	z				0						0		
M2	x				0.5						0.5		
	y				0						0		
	z				0.5						0.5		
Si	x	0.960(2)	0.962(1)	0.966(2)	0.966(1)	0.964(1)	0.9653(7)	0.9651(8)	0.9651(6)	0.9653(8)	0.9668(7)	0.9661(9)	0.9657(8)
	y	0.1324(5)	0.1314(3)	0.1324(6)	0.1332(3)	0.1319(2)	0.1315(2)	0.1311(2)	0.1314(2)	0.1298(2)	0.1298(2)	0.1297(2)	0.1305(2)
	z	0.980(2)	0.979(1)	0.983(2)	0.986(1)	0.987(1)	0.9880(6)	0.9888(7)	0.9891(5)	0.9892(7)	0.9905(7)	0.9902(8)	0.9908(8)
O1	x	0.927(5)	0.929(3)	0.926(5)	0.928(3)	0.934(3)	0.937(2)	0.948(2)	0.935(2)	0.951(2)	0.945(2)	0.954(3)	0.940(2)
	y				0.75						0.75		
	z	0.957(6)	0.947(3)	0.957(5)	0.941(3)	0.942(3)	0.939(2)	0.939(2)	0.936(2)	0.938(2)	0.936(2)	0.938(2)	0.931(2)
O2	x	0.764(4)	0.764(2)	0.760(4)	0.760(2)	0.762(2)	0.761(1)	0.767(2)	0.764(1)	0.772(2)	0.770(1)	0.771(2)	0.768(2)
	y	0.114(2)	0.116(6)	0.115(2)	0.1148(7)	0.1155(7)	0.1149(4)	0.1126(5)	0.1137(3)	0.1104(5)	0.1107(5)	0.1104(5)	0.1104(5)
	z	0.653(5)	0.653(2)	0.653(4)	0.661(2)	0.656(2)	0.658(1)	0.663(2)	0.659(1)	0.665(2)	0.662(2)	0.665(2)	0.661(2)
O3	x	0.777(5)	0.779(2)	0.765(4)	0.778(2)	0.774(3)	0.776(1)	0.783(2)	0.780(1)	0.790(2)	0.788(2)	0.788(2)	0.788(2)
	y	0.389(2)	0.3862(7)	0.388(2)	0.3915(7)	0.3894(7)	0.3914(4)	0.3936(5)	0.3934(3)	0.3971(5)	0.3977(5)	0.3980(5)	0.3967(5)
	z	0.126(5)	0.115(2)	0.106(4)	0.118(2)	0.120(2)	0.118(1)	0.124(2)	0.121(1)	0.125(2)	0.123(2)	0.126(2)	0.127(2)
O4	x	0.280(4)	0.291(2)	0.278(4)	0.280(2)	0.280(3)	0.285(2)	0.289(2)	0.287(1)	0.294(2)	0.292(2)	0.293(2)	0.289(2)
	y	0.068(1)	0.0660(6)	0.068(1)	0.0687(6)	0.0688(6)	0.0686(4)	0.0704(5)	0.0698(3)	0.0725(4)	0.0723(4)	0.0726(5)	0.0722(4)
	z	0.143(5)	0.146(2)	0.143(4)	0.142(2)	0.137(2)	0.141(1)	0.145(2)	0.141(1)	0.149(2)	0.146(2)	0.146(2)	0.144(2)
O5	x	0.276(5)	0.282(2)	0.275(3)	0.277(2)	0.280(2)	0.282(1)	0.287(2)	0.285(1)	0.293(2)	0.290(2)	0.292(2)	0.291(2)
	y	0.054(1)	0.0535(6)	0.054(1)	0.0548(7)	0.0544(6)	0.0542(4)	0.0554(5)	0.0546(3)	0.0561(4)	0.0554(4)	0.0552(5)	0.0567(5)
	z	0.636(4)	0.638(2)	0.633(4)	0.638(2)	0.638(2)	0.637(1)	0.643(2)	0.640(1)	0.641(2)	0.642(2)	0.642(2)	0.642(2)
O6	x	0.760(5)	0.774(3)	0.764(5)	0.770(3)	0.762(4)	0.758(2)	0.742(2)	0.750(2)	0.732(2)	0.732(2)	0.736(2)	0.730(2)
	y				0.75						0.75		
	z	0.348(6)	0.352(3)	0.358(5)	0.349(3)	0.340(4)	0.329(2)	0.306(2)	0.319(2)	0.291(2)	0.291(2)	0.293(2)	0.290(2)

Notes: Refinements in space group $P2_1/m$. $Z = 2$; errors in parentheses refer to 2σ, x_{Sr} based on XRD.

TABLE 4b. Fractional atomic coordinates of orthorhombic (Ca-Sr)-lawsonite

Run		Au76	Au77	Au78	Au79	Au63	Au62	Au83	Au86
x_{Sr}		0.018(12)	0.029(12)	0.035(18)	0.021(12)	0.111(43)	0.193(3)	0.18(4)	
A	x				0				
	y	0.3337(3)	0.3320(3)	0.3328(4)	0.3323(4)	0.3330(8)	0.3320(8)	0.3312(8)	0.307(4)
	z				0.25				
M	x				0.25				
	y				0.25				
	z				0				
Si	x				0				
	y	0.9810(3)	0.9805(3)	0.9809(4)	0.9799(4)	0.9824(8)	0.9820(9)	0.9808(8)	0.956(4)
	z	0.1329(2)	0.1332(2)	0.1330(2)	0.1322(2)	0.1333(6)	0.1365(5)	0.1324(5)	0.134(3)
O1	x				0				
	y	0.0484(9)	0.0481(9)	0.048(1)	0.046(1)	0.051(2)	0.044(2)	0.049(2)	0.05(1)
	z				0.25				
O2	x	0.2734(7)	0.2725(7)	0.2726(7)	0.2707(8)	0.275(1)	0.272(2)	0.271(2)	0.258(7)
	y	0.3796(5)	0.3796(5)	0.3796(5)	0.3793(5)	0.377(1)	0.381(1)	0.381(1)	0.310(7)
	z	0.1175(3)	0.1171(2)	0.1175(3)	0.1162(3)	0.1199(8)	0.1143(7)	0.1175(8)	0.142(3)
O3	x				0				
	y	0.1390(7)	0.1387(7)	0.1384(8)	0.1401(8)	0.139(2)	0.136(2)	0.142(2)	0.125(9)
	z	0.0651(4)	0.0652(4)	0.0652(4)	0.0676(4)	0.064(1)	0.070(1)	0.066(1)	0.057(5)
O4	x				0				
	y	0.6391(6)	0.6401(6)	0.6395(7)	0.6359(7)	0.642(2)	0.640(2)	0.641(2)	0.595(8)
	z	0.0487(4)	0.0492(4)	0.0489(4)	0.0507(5)	0.049(1)	0.051(1)	0.049(1)	0.044(5)
O5	x				0				
	y	0.609(1)	0.608(1)	0.608(1)	0.604(1)	0.606(2)	0.627(3)	0.610(3)	0.66(2)
	z				0.25				

Notes: Refinements in space group *Cmcm*. $Z = 4$; errors in parentheses refer to 2σ, x_{Sr} based on XRD.

increase linearly with increasing x_{Sr}. The A site in orthorhombic lawsonite is generally eightfold coordinated and its mean bond length slightly increases with increasing x_{Sr}.

Octahedra. The individual octahedra are almost unaffected by incorporation of Sr in both polymorphs. Individual M-O bond lengths are independent on x_{Sr} and the mean M-O bond lengths are constant in all runs and range between 1.91 and 1.93 Å.

Si_2O_7-group. Bond lengths and interatomic angles of the tetrahedra scatter in both polymorphs without any compositional dependency. The mean bond lengths are comparable in both polymorphs. Both polymorphs, however, differ with respect to the tilting of the individual tetrahedra within the Si_2O_7-group (Fig. 6b)—in monoclinic lawsonite, the T-O1-T angle increases linearly from 144.3 to 152.0° with increasing x_{Sr} whereas O4-O1-O4 decreases linearly from 138.8 to 128.5°. Extrapolation to Ca end-member composition yields T-O1-T = 143.3° and O4-O1-O4 = 140.6°, which are larger, respectively, smaller than the corresponding 138 and 143° in orthorhombic lawsonite. O2-

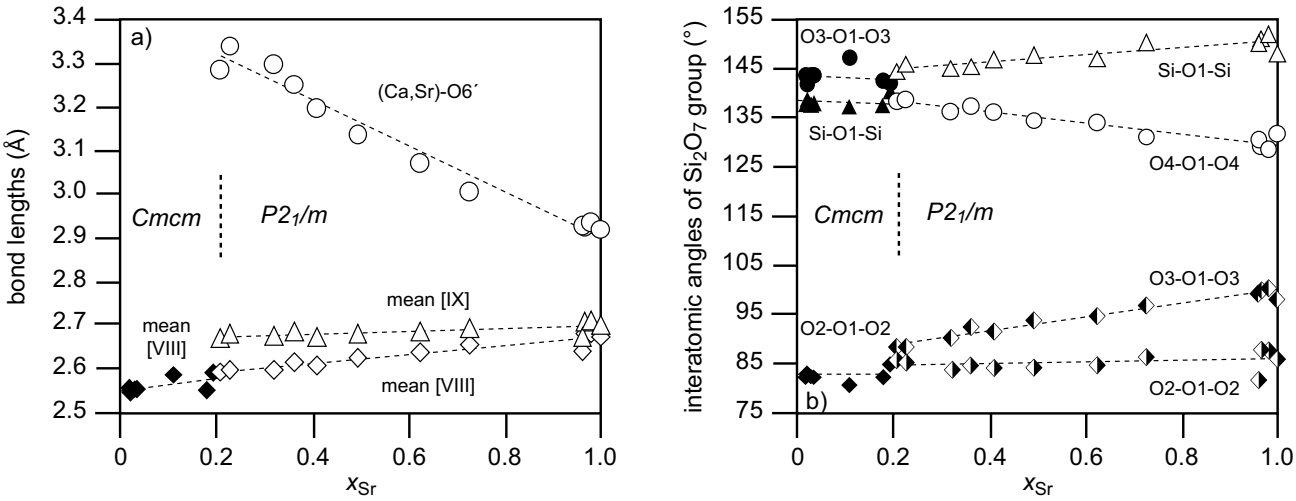

FIGURE 6. (**a**) Mean bond lengths of A sites in orthorhombic (filled diamonds = eightfold coordination) and monoclinic (Ca,Sr)-lawsonite (open diamonds = eightfold coordination, open triangles = ninefold coordination) and distance of A site to O6′ in monoclinic lawsonite. Due to the decreasing (Ca,Sr)-O6′ distance, the A site in monoclinic (Ca,Sr)-lawsonite is best described as ninefold coordinated at high x_{Sr}. (**b**) Tilting of the individual tetrahedra of the Si_2O_7-group in orthorhombic (filled symbols) and monoclinic (Ca,Sr)-lawsonite (open and half-filled symbols).

O1-O2 is only slightly larger in monoclinic than in orthorhombic lawsonite and relatively unaffected by Sr-incorporation in both polymorphs, while O3-O1-O3 of monoclinic lawsonite linearly increases with increasing x_{Sr}. Extrapolation to Ca end-member composition yields 86.1°, larger than the corresponding O2-O1-O2 of ~82.5° in orthorhombic lawsonite.

DISCUSSION

(Ca,Sr)-lawsonite solid-solution series and effect of Sr on lawsonite stability

Orthorhombic lawsonite could be synthesized up to x_{Sr}^{ortho} = 0.19, while monoclinic lawsonite could be synthesized with x_{Sr}^{mono} = 0.21 to 1.0. Given the stability of monoclinic Ca end-member lawsonite at high pressure (Daniel et al. 2000; Pawley and Allan 2001; Boffa-Ballaran and Angel 2003) and the natural occurrence of orthorhombic Sr end-member itoigawaite (Miyajima et al. 1999), our data strongly suggest complete Ca-Sr solid-solutions series in both polymorphs at appropriate *P-T* conditions. The synthesis of orthorhombic lawsonite at low x_{Sr}^{bulk} vs. monoclinic lawsonite at higher x_{Sr}^{bulk} in our runs reflects a change in relative stability between both polymorphs in *P-T-x* space and the existence of an orthorhombic-monoclinic two-phase field. The exact compositional limits of this two-phase field can, however, not be determined precisely: (1) A divariant two-phase field implies fixed compositions of coexisting orthorhombic and monoclinic lawsonite, which are independent on bulk composition. This is not the case for runs Au62, Au63, and Au83, in which x_{Sr} of orthorhombic lawsonite varies between 0.11 and 0.19 and that of coexisting monoclinic lawsonite between 0.21 and 0.32. But in line with such a two-phase field, the modal amount of orthorhombic lawsonite decreases in favor of monoclinic lawsonite from 42% at x_{Sr}^{bulk} = 0.18 to 6% at x_{Sr}^{bulk} = 0.4. (2) The lattice parameters and also some fractional atom coordinates for monoclinic lawsonite at $x_{Sr}^{bulk} \leq 0.4$ deviate from the linear trends defined by monoclinic lawsonite at $x_{Sr}^{bulk} > 0.4$. This makes especially the compositional data for these runs less reliable. Combining the observed compositional ranges of coexisting orthorhombic and monoclinic lawsonite with the only minor amount of orthorhombic lawsonite at x_{Sr}^{bulk} = 0.4 and its lack in runs at $x_{Sr}^{bulk} > 0.4$, our data nevertheless suggest compositional limits for the two-phase field of x_{Sr}^{ortho} = 0.1 to 0.2 and x_{Sr}^{mono} = 0.3 to 0.4 at 4 GPa/600 °C.

Any discussion on the effects of Sr on the stability of lawsonite is hampered by the fact that we only performed synthesis experiments without bracketing approaches. We therefore cannot rule out metastable formation of (Ca,Sr)-lawsonite in the runs. However, synthesis of the Sr end-member at 800 °C/4 GPa allows for some speculations. The upper thermal stability of lawsonite within the CASH system at 4 GPa is defined by the reaction

lawsonite = kyanite + zoisite + coesite + H_2O.

Within CASH, experimental data indicate that this breakdown of lawsonite occurs at 777 ± 3 °C (Skrok 1993; Poli and Schmidt 1998) at 4 GPa, 20 to 25 °C below our synthesis temperature for Sr end-member lawsonite. Our data, therefore, suggest that adding Sr to the CASH system enlarges the stability field of lawsonite. This interpretation is also supported by the observed fractionation of Sr into lawsonite compared to zoisite but also grossular and margarite (Dörsam et al. 2007a, 2007b; Liebscher et al. 2009) thus stabilizing lawsonite vs. these minerals.

Structural effects caused by Sr-incorporation vs. effects caused by *P* and *T*

In monoclinic lawsonite, mainly tilting and rotation of the individual polyhedra compensate the substitution of the larger Sr for Ca; only the A site itself increases in size. The rotation of the individual tetrahedra of the Si_2O_7 group leads to shearing of $(100)_{mono}$ in $[001]_{mono}$ with increasing deviation of $(O3\text{-}O1\text{-}O3)_{mono}$ from $(O2\text{-}O1\text{-}O2)_{mono}$ (see Figs. 1 and 6). However, symmetry restrictions forbid this type of polyhedra rotation and splitting of $O2_{ortho}$ into O2 and O3 with independent shifts of O3 and O2 in orthorhombic lawsonite. Here, a notable increase of c_{ortho} mainly

compensates the substitution of the larger Sr for Ca and leads to a more pronounced overall expansion of the orthorhombic compared to the monoclinic structure (see Fig. 5c). These different expansion mechanisms in monoclinic and orthorhombic lawsonite explain the increasing structural differences between both polymorphs with increasing x_{Sr} as indicated by our data. Especially the increasingly negative $\Delta v_{ortho\text{-}mono}$ with increasing x_{Sr} is responsible for the notable shift of the *Cmcm* to $P2_1/m$ phase transition to lower pressure in the Sr-bearing system (see below).

Taking our extrapolated lattice parameters for the monoclinic Ca end-member as a_0, b_0, and c_0, we calculate the relative compressibility of a_{mono}, b_{mono}, and c_{mono} using the monoclinic high-*P* data of Pawley and Allan (2001; Fig. 7a); the relative compressibility increases in the order $a < b < c$. No thermal expansion data are available for monoclinic Ca-lawsonite. However, structural effects of increasing temperature are often opposite to those of increasing pressure. One may therefore speculate that $\alpha_a < \alpha_b < \alpha_c$ in monoclinic Ca-lawsonite. The relative expansion of the lattice parameters in monoclinic (Ca,Sr)-lawsonite solid solutions with increasing x_{Sr} as determined here (Fig. 7b) is, however, $c < b < a$. In orthorhombic Ca-lawsonite, deformation during isothermal compression is almost isotropic although the order of relative compressibility varies in the different studies: Holland et al. (1996) and Pawley and Allan (2001) determined $\beta_c < \beta_b \sim \beta_a$, Grevel et al. (2000) determined $\beta_a < \beta_c < \beta_b$, while Comodi and Zanazzi (1996) determined $\beta_c < \beta_a < \beta_b$. The isobaric thermal expansion of orthorhombic Ca-lawsonite is likewise nearly isotropic with $\alpha_c < \alpha_b \sim \alpha_a$ (Comodi and Zanazzi 1996; Pawley et al. 1996). The relative change of lattice parameters in orthorhombic (Ca,Sr)-lawsonite solid solutions with increasing x_{Sr} as determined here is, however, $a < c \sim b$. The data therefore indicate that the structural changes in monoclinic and orthorhombic lawsonite due to incorporation of Sr differ from those induced by pressure and temperature.

There are, however, also similarities between the effects caused by x_{Sr} and those caused by pressure and temperature. Ninefold coordination of the A site due to a second O6 was also observed by Pawley and Allan (2001) in monoclinic, high-*P*, Ca end-member lawsonite. The observed increase of T-O1-T in monoclinic lawsonite due to the incorporation of the larger Sr for Ca is equivalent to the increase of T-O1-T in orthorhombic Ca end-member lawsonite due to thermal expansion determined by Comodi and Zanazzi (1996) and opposite to the decrease of T-O1-T in orthorhombic and monoclinic Ca end-member due to isothermal compression, where $(T\text{-}O1\text{-}T)_{ortho}$ decreases to 130.7° at 8.9 GPa, and $(T\text{-}O1\text{-}T)_{mono}$ decreases to 104.7° at 11.9 GPa (Pawley and Allan 2001). This indicates that the Si_2O_7-group serves as a structural hinge and that its tilting allows for contraction or expansion of the structure due to either compositional changes or to changes in pressure and temperature.

PVTx behavior of (Ca,Sr)-lawsonite

Bulk modulus of monoclinic Ca-lawsonite. High-pressure volume data for monoclinic Ca-lawsonite are available from Daniel et al. (2000) and Pawley and Allan (2001). Due to the

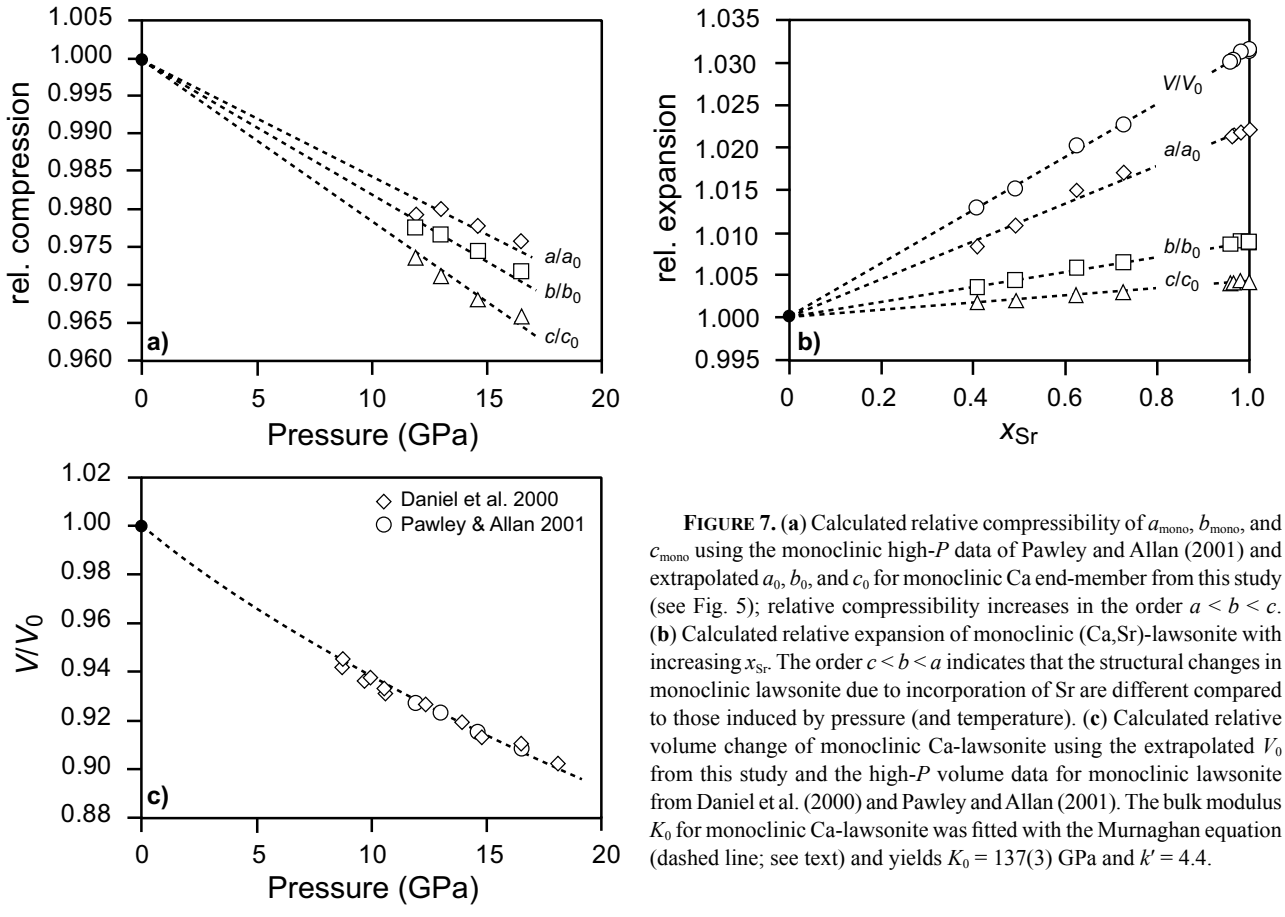

FIGURE 7. (**a**) Calculated relative compressibility of a_{mono}, b_{mono}, and c_{mono} using the monoclinic high-*P* data of Pawley and Allan (2001) and extrapolated a_0, b_0, and c_0 for monoclinic Ca end-member from this study (see Fig. 5); relative compressibility increases in the order $a < b < c$. (**b**) Calculated relative expansion of monoclinic (Ca,Sr)-lawsonite with increasing x_{Sr}. The order $c < b < a$ indicates that the structural changes in monoclinic lawsonite due to incorporation of Sr are different compared to those induced by pressure (and temperature). (**c**) Calculated relative volume change of monoclinic Ca-lawsonite using the extrapolated V_0 from this study and the high-*P* volume data for monoclinic lawsonite from Daniel et al. (2000) and Pawley and Allan (2001). The bulk modulus K_0 for monoclinic Ca-lawsonite was fitted with the Murnaghan equation (dashed line; see text) and yields $K_0 = 137(3)$ GPa and $k' = 4.4$.

restricted P-range analyzed and the lack of V_0 data for monoclinic lawsonite, these authors did not determine the bulk modulus of monoclinic lawsonite. We use our extrapolated monoclinic Ca-lawsonite volume of 337.58 Å^3 at room temperature as V_0 and combine it with the volume data for monoclinic lawsonite from Daniel et al. (2000) and Pawley and Allan (2001) to determine the bulk modulus K_0 for monoclinic Ca-lawsonite (Fig. 7c). The data were fitted with a Murnaghan equation $V/V_0 = (1 + K'/K_0 \cdot P)^{-1/k'}$ minimizing $\{[(V/V_0^{obs}) - (V/V_0^{calc})]/(V/V_0^{obs})\}^2$. The resulting bulk modulus for monoclinic lawsonite is K_0 = 137(3) GPa with K' = 4.4 (Fig. 7c). This value is higher than K_0 for orthorhombic lawsonite, which has been determined to 96 GPa (Comodi and Zanazzi 1996), 107 GPa (Grevel et al. 2000), 112 GPa (Chinnery et al. 2000), 124 GPa (Daniel et al. 2000), 126 GPa (Pawley and Allan 2001), and 191 GPa (Holland et al. 1996). Excluding the last value, which is probably too high due to some experimental problems (see discussion in Pawley and Allan 2001), the range of 96 and 126 GPa for K_0 of orthorhombic Ca-lawsonite indicates a lower compressibility of monoclinic lawsonite, consistent with the results of Daniel et al. (2000).

***Cmcm–P2$_1$/m* phase transition.** While the orthorhombic to monoclinic phase transition is reversible and non-quenchable in the Ca end-member system, it is clearly reconstructive and quenchable within the Sr-bearing system. Despite the general problems associated with interpretation of synthesis results, our data in combination with published in situ data (Comodi and Zanazzi 1996; Pawley et al. 1996; Chinnery et al. 2000; Daniel et al. 2000; Grevel et al. 2000; Pawley and Allan 2001) and the natural occurrence of orthorhombic Sr end-member itoigawaite (Miyajima et al. 1999) allow for some general conclusions regarding the *Cmcm–P*2$_1$/*m* phase transition (Fig. 8). Within the Ca end-member system, the *Cmcm–P*2$_1$/*m* phase transition occurs at room temperature between ~8.5 and ~11.0 GPa (Daniel et al. 2000; Pawley and Allan 2001). The phase transition has not yet been determined at higher temperature; however, Pawley and Allan (2001) found monoclinic Ca-lawsonite stable up to ~11.2 GPa/200 °C, while Grevel et al. (2000) and Chinnery et al. (2000) found orthorhombic Ca-lawsonite stable up to ~7 GPa/800 °C and 7 GPa/600 °C. At atmospheric pressure, orthorhombic Ca-lawsonite does not decompose at least up to 590 °C and does not transform into the monoclinic form (Pawley et al. 1996). These data place some constraints on the *P-T* location of the *Cmcm–P*2$_1$/*m* phase transition in the Ca-system: the slope is very flat, undetermined from slightly negative with –0.004 GPa/K to

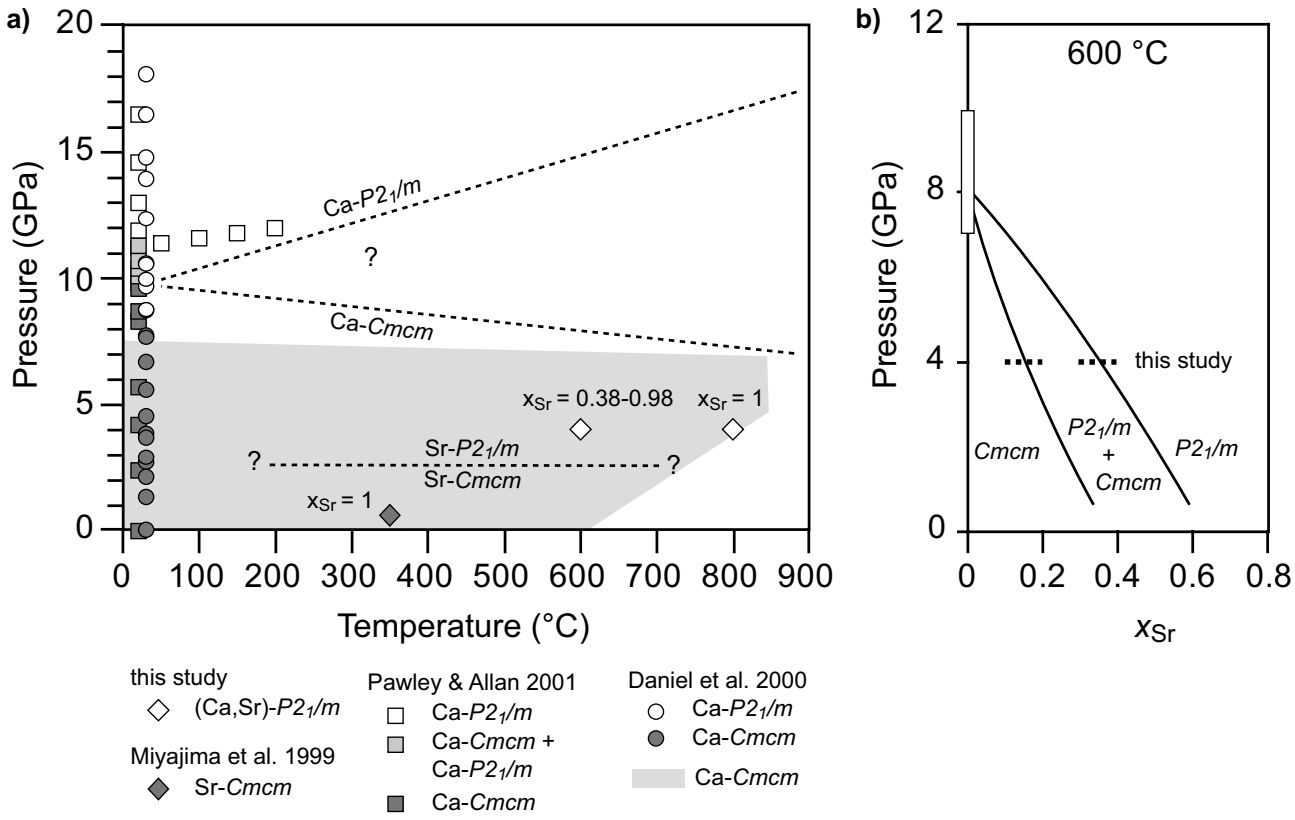

Figure 8. (**a**) Stability fields of orthorhombic and monoclinic lawsonite Ca end-members as compiled from the literature [shadowed field for Ca-*Cmcm* lawsonite refers to data by Comodi and Zanazzi (1996), Pawley et al. (1996), Chinnery et al. (2000), and Grevel et al. (2000)]. The *P-T* conditions for natural itoigawaite (Miyajima et al. 1999; Morishita 2005) and synthesis conditions for monoclinic (Ca,Sr)-lawsonite from this study are shown for comparison. The Ca-*Cmcm*–Ca-*P*2$_1$/*m* transition at room temperature occurs at ~10 GPa and has a flat slope (not exactly determined but most probably slightly negative, see text). The combined data suggest that in the Sr-system the Sr-*Cmcm*–Sr-*P*2$_1$/*m* transition occurs at much lower pressure between 1 and <4 GPa. (**b**) Tentative schematic *P*-x_{Sr} diagram showing the stability fields of orthorhombic and monoclinic (Ca,Sr)-lawsonite and the orthorhombic + monoclinic two-phase field. Diagram drawn for 600 °C based on the results of this study for x_{Sr} of coexisting orthorhombic and monoclinic (Ca,Sr)-lawsonite (thick dotted lines) and assuming a negative slope for the Ca-*Cmcm*–Ca-*P*2$_1$/*m* transition, resulting in P ~ 7 to 10 GPa at 600 °C (white box).

slightly positive with +0.006 GPa/K (Fig. 8). Given the lower symmetry of monoclinic lawsonite and the splits of $O2_{ortho}$ into $O2_{mono}$ and $O3_{mono}$ and of $M1_{ortho}$ into $M1_{mono}$ and $M2_{mono}$, one may speculate on an increase of entropy and a positive $\Delta S_{ortho\text{-}mono}$ for the *Cmcm*–$P2_1/m$ phase transition. Combined with the negative $\Delta V_{ortho\text{-}mono}$ this suggests a negative slope for the *Cmcm*–$P2_1/m$ phase transition as most plausible. But regardless of the actual *P-T* slope of the Ca end-member transition, the data show that monoclinic (Ca,Sr)-lawsonite of this study was synthesized well within the stability field of orthorhombic Ca-lawsonite as indicated by the previous studies. This implies that incorporation of Sr expands the stability field of monoclinic lawsonite toward lower pressure. Such a shift of the phase transition with x_{Sr} to lower pressure is also consistent with the observed increase in volume difference between orthorhombic and monoclinic lawsonite with increasing x_{Sr}. Assuming a negative slope for the Ca-*Cmcm*–Ca-$P2_1/m$ phase transition and a minimum pressure stability of orthorhombic Ca-lawsonite as determined by Grevel et al. (2000) and Chinnery et al. (2000), the data indicate ~7 to 10 GPa at 600 °C for the Ca-*Cmcm*–Ca-$P2_1/m$ phase transition. Taking this pressure range and the results of this study for the composition of coexisting orthorhombic and monoclinic (Ca,Sr)-lawsonite at 4 GPa/600 °C, we constructed a tentative orthorhombic-monoclinic (Ca,Sr)-lawsonite phase diagram at 600 °C (Fig. 8b). The resulting two-phase field is quite narrow and shifts significantly to lower pressure with increasing x_{Sr}. Combining this phase diagram with the formation conditions of natural itoigawaite of ~0.6 GPa/350 °C (Miyajima et al. 1999; Morishita 2005) implies that also the Sr-*Cmcm*–Sr-$P2_1/m$ phase transition has a negative slope and is located at ≤1 GPa at ~400 to 600 °C, i.e., 6 to 9 GPa below the transition in the Ca-system. The exact *P-T* slopes of the *Cmcm*–$P2_1/m$ phase transition in the Ca and Sr end-member systems as well as the exact shape of the orthorhombic-monoclinic two-phase field cannot be determined with the data at hand.

ACKNOWLEDGMENTS

This work was supported by the DFG grant no. FR557/18. We thank F. Galbert (ZELMI, TU Berlin) for his help at the electron microprobe, C. Zecha (TU Berlin) for the polished grain mounts, and S. Steigert and A. Hahn (GFZ Potsdam) for help with the XRD. Helpful and constructive reviews by S. Poli and A. Pawley improved the manuscript and are gratefully acknowledged.

REFERENCES CITED

Armbruster, T., Oberhänsli, R., and Bermanec, V. (1992) Crystal structure of $SrMn_2[Si_2O_7](OH)_2 \cdot H_2O$, a new mineral of the lawsonite type. European Journal of Mineralogy, 4, 17–22.

Baur, W.H. (1978) Crystal structure refinement of lawsonite. American Mineralogist, 63, 311–315.

Boffa-Ballaran, T. and Angel, R.J. (2003) Equation of state and high-pressure phase transitions in lawsonite. European Journal of Mineralogy, 15, 241–246.

Caglioti, G., Paoletti, A., and Ricci, F.P. (1958) Choice of collimators for a crystal spectrometer for neutron diffraction. Nuclear Instruments, 3, 223–228.

Chinnery, N., Pawley, A.R., and Clark, S.M. (2000) The equation of state of lawsonite to 7 GPa and 873 K, and calculation of its high pressure stability. American Mineralogist, 85, 1001–1008.

Comodi, P. and Zanazzi, P.F. (1996) Effects of temperature and pressure on the structure of lawsonite. American Mineralogist, 81, 833–841.

Daniel, I., Fiquet, G., and Gillet, P. (2000) High-pressure behaviour of lawsonite: A phase transition at 8.6 GPa. European Journal of Mineralogy, 12, 721–733.

Dörsam, G., Liebscher, A., Wunder, B., Franz, G., and Gottschalk, M., (2007a) Crystal chemistry of synthetic $Ca_2Al_3Si_3O_{12}OH$–$Sr_2Al_3Si_3O_{12}OH$ solid-solution series of zoisite and clinozoisite. American Mineralogist, 92, 1133–1147.

Dörsam, G., Liebscher, A., Wunder, B., Gottschalk, M., and Franz, G. (2007b) Experimental determination of Ca-Sr distribution between zoisite-fluid and lawsonite-fluid. Geochimica et Cosmochimica Acta, 71, Supplement 1, A228.

Grevel, K.-D., Nowlan, E.U., Fasshauer, D.W., and Burchard, M. (2000) In situ X-ray diffraction investigation of lawsonite and zoisite at high pressures and temperatures. American Mineralogist, 85, 206–216.

Holland, T.J.B., Redfern, S.A.T., and Pawley, A.R. (1996) Volume behavior of hydrous minerals at high pressure and temperature: II. Compressibilities of lawsonite, zoisite, clinozoisite, and epidote. American Mineralogist, 81, 341–348.

Kawachi, Y., Coombs, D.S., and Miura, H. (1996) Noelbensonite, a new BaMn silicate of the lawsonite structure type, from Woods Mine, New South Wales, Australia. Mineralogical Magazine, 60, 369–374.

Larson, A.C. and Von Dreele, R.B. (1987) General Structure Analysis System (GSAS). Los Alamos National Laboratory, New Mexico, Report LAUR 86-748.

Libowitzky, E. and Armbruster, Th. (1995) Low-temperature phase transitions and the role of hydrogen bonds in lawsonite. American Mineralogist, 80, 1277–1285.

Libowitzky, E. and Rossman, G.R. (1996) FTIR spectroscopy of lawsonite between 82 and 325 K. American Mineralogist, 81, 1080–1091.

Liebscher, A., Thiele, M., Franz, G., Dörsam, G., and Gottschalk, M. (2009) Synthetic Sr–Ca margarite, anorthite and slawsonite solid solutions and solid–fluid Sr–Ca fractionation. European Journal of Mineralogy, 21, 275–292.

Martin-Olalla, J.M., Haywards, S.A., Meyer, H.M., Ramos, S., Cerro, J., and Carpenter, M.A. (2001) Phase transitions in lawsonite. European Journal of Mineralogy, 13, 5–14.

Meyer, H.W., Marion, S., Sondergeld, P., Carpenter, M.A., Knight, K.S., Redfern, S.A.T., and Dove, M.T. (2001) Displacive components of the low-temperature phase transitions in lawsonite. American Mineralogist, 86, 566–577.

Meyer, H.W., Carpenter, M.A., Graeme-Barber, A., Sondergeld, P., and Schranz, W. (2000) Local and macroscopic order parameter variations associated with low temperature phase transitions in lawsonite, $CaAl_2Si_2O_7(OH)_2 \cdot H_2O$. European Journal of Mineralogy, 12, 1139–1150.

Miyajima, H., Matsubara, S., Miyawaki, R., and Ito, K. (1999) Itoigawaite, a new mineral, the Sr analogue of lawsonite, in jadeitite from the Itoigawa-Ohmi District, central Japan. Mineralogical Magazine, 63, 909–916.

Morishita, T. (2005) Occurrence and chemical composition of barian feldspars in a jadeitite from the Itoigawa-Ohmi district in the Renge high-*P/T*-type metamorphic belt, Japan. Mineralogical Magazine, 69, 39–51.

Pawley, A.R. and Allan, D.R. (2001) A high-pressure study of lawsonite using angle-dispersive powder-diffraction methods with synchrotron radiation. Mineralogical Magazine, 65, 41–58.

Pawley, A.R., Redfern, S.A.T., and Holland, T.J.B. (1996) Volume behavior of hydrous minerals at high pressure and temperature: I. Thermal expansion of lawsonite, zoisite, clinozoisite, and diaspore. American Mineralogist, 81, 335–340.

Poli, S. and Schmidt, M.W. (1998) The high-pressure stability of zoisite and phase relationships of zoisite-bearing assemblages. Contributions to Mineralogy and Petrology, 130, 162–175.

Pouchou, J.L. and Pichoir, F. (1984) Un nouveau modèle de calcul pour la microanalyse quantitative par spectrométrie de rayons X. La Recherche Aérospatiale, 3, 167–192.

Schmidt, M.W. (1995) Lawsonite: Upper pressure stability and formation of higher density hydrous phases. American Mineralogist, 80, 1286–1292.

Scott, H.P. and Williams, Q. (1999) An infrared spectroscopic study of lawsonite to 20 GPa. Physics and Chemistry of Minerals, 26, 437–445.

Skrok, V. (1993) Synthese und Stabilität von Lawsonit im System CaO-Al_2O_3-SiO_2-H_2O unter hohen Drücken [translated title: Synthesis and stability of lawsonite in the system CaO-Al_2O_3-SiO_2-H_2O at high pressures], 51 p. Diploma thesis, Ruhr-Universität Bochum, Germany.

Spandler, C., Hermann, J., and Arculus, R. (2003) Redistribution of trace elements during prograde metamorphism from lawsonite blueschist to eclogite facies; implications for deep subduction-zone processes. Contributions to Mineralogy and Petrology, 146, 205–222.

Tribuzio, R., Messiga, B., Vannucci, R., and Bottazzi, P. (1996) Rare earth element redistribution during high-pressure–low-temperature metamorphism in ophiolitic Fe-gabbros (Liguria, northwestern Italy): Implications for light REE mobility in subduction zones. Geology, 24, 711–714.

Zack, T., Foley, S.F., and Rivers, T. (2002) Equilibrium and disequilibrium trace element partitioning in hydrous eclogites (Trescolmen, Central Alps). Journal of Petrology, 43, 1947–1974.

Zimmermann, R., Heinrich, W., and Franz, G. (1996) Tremolite synthesis from $CaCl_2$-bearing aqueous solutions. European Journal of Mineralogy, 8, 767–776.

MANUSCRIPT RECEIVED FEBRUARY 17, 2009
MANUSCRIPT ACCEPTED DECEMBER 14, 2009
MANUSCRIPT HANDLED BY AARON CELESTIAN